ESC HEART FAILURE
ESC Heart Failure 2021; **8**: 447–460
Published online 24 November 2020 in Wiley Online Library (wileyonlinelibrary.com) **DOI:** 10.1002/ehf2.13095

ORIGINAL RESEARCH ARTICLE

Crosstalk between the activated Slit2–Robo1 pathway and TGF-β1 signalling promotes cardiac fibrosis

Yunqi Liu[1,2†], Ziwei Yin[3†], Xueqin Xu[1,2], Chen Liu[2,4], Xiaoying Duan[1,2], Qinlan Song[1,2], Ying Tuo[5], Cuiping Wang[6], Jing Yang[7*] and Shengli Yin[1,2*]

[1]*Department of Cardiac Surgery, The First Affiliated Hospital, Sun Yat-sen University, Guangzhou, China;* [2]*NCH Key Laboratory of Assisted Circulation, Sun Yat-sen University, Guangzhou, China;* [3]*Division of Biosciences, University College London, London, UK;* [4]*Department of Cardiology, The First Affiliated Hospital, Sun Yat-sen University, Guangzhou, China;* [5]*Department of Pathology, The First Affiliated Hospital, Sun Yat-sen University, Guangzhou, China;* [6]*Department of Cardiothoracic Surgery ICU, The First Affiliated Hospital, Sun Yat-sen University, Guangzhou, China;* [7]*Department of Pediatric Dentistry, Stomatological Hospital, Southern Medical University, Guangzhou, China*

Abstract

Aims Previous reports indicated that the Slit2–Robo signalling pathway is involved in embryonic heart development and fibrosis in other solid organs, but its function in adult cardiac fibrosis has not been investigated. Here, we investigate the role of the Slit2–Robo1 signalling pathway in cardiac fibrosis.

Methods and results The right atrial tissue samples were obtained from patients with valvular heart disease complicated by atrial fibrillation during heart valve surgery and from healthy heart donors. The fibrotic animal model is created by performing transverse aortic constriction (TAC) surgery. The Robo1, Slit2, TGF-β1, and collagen I expression levels in human and animal samples were evaluated by immunohistochemistry and western blot analysis. Echocardiography measured the changes in heart size and cardiac functions of animals. Angiotensin II (Ang II), *Slit2-siRNA*, *TGF-β1-siRNA*, recombinant Slit2, and recombinant TGF-β1 were transfected to cardiac fibroblasts (CFs) respectively to observe their effects on collagen I expression level. The right atrial appendage of patients with valvular heart disease complicated by atrial fibrillation found significantly up-regulated Slit2, Robo1, TGF-β1, and collagen I expression levels. TAC surgery leads to heart enlargement, cardiac fibrosis, and up-regulation of Slit2, Robo1, TGF-β1, and collagen I expression levels in animal model. Robo1 antagonist R5 and TGF-β1 antagonist SB431542 suppressed cardiac fibrosis in TAC mice. Treatment with 100 nM Ang II in CFs caused significantly increased Slit2, Robo1, Smad2/3, TGF-β1, collagen I, PI3K, and Akt expression levels. Transfecting *Slit2-siRNA* and *TGF-β1-siRNA*, respectively, into rat CFs significantly down-regulated Smad2/3 and collagen I expression, inhibiting the effects of Ang II. Recombinant Slit2 activated the TGF-β1/Smad signalling pathway in CFs and up-regulated Periostin, Robo1, and collagen I expression.

Conclusions The Slit2–Robo1 signalling pathway interfered with the TGF-β1/Smad pathway and promoted cardiac fibrosis. Blockade of Slit2–Robo1 might be a new treatment for cardiac fibrosis.

Keywords Cardiac fibrosis; Slit2; TGF-β1; Signalling pathway; Crosstalk

Received: 8 June 2020; Revised: 27 September 2020; Accepted: 22 October 2020
**Correspondence to: Shengli Yin, Department of Cardiac Surgery, The First Affiliated Hospital, Sun Yat-sen University, No.58, Zhongshan Road II, Guangzhou 510080, China. Tel: +86 13922273098; Fax: +86 020-87333122. Email: yshengl03@163.com*
Jing Yang, Department of Pediatric Dentistry, Stomatological Hospital, Southern Medical University, No. 366, South Jiangnan Avenue, Guangzhou 510280, China. Tel: +86 18928801580. Email: yjgirl2@163.com
†Liu Yunqi and Ziwei Yin contributed equally to this work.

Introduction

Heart failure (HF) remains a major cause of mortality and poor quality of life and has become an increasing threat to global health.[1] During HF, multiple pathogenic factors can exacerbate adverse cardiac remodelling and fibrosis, leading to further cardiac contractile function loss and arrhythmias.[2] Therefore, understanding the currently understudied molecular mechanism of cardiac fibrosis is key to discovering potential treatments for many cardiac diseases.

The pathogenesis of cardiac fibrosis includes disruption of normal myocardial construction and abnormal extracellular matrix (ECM) accumulation.[3] The key pathophysiological basis is the feedback cycle between HF and continuous differentiation of cardiac fibroblasts (CFs) into cardiac myofibroblasts,[4] which have a potent ability to divide and cause ECM overproduction.[5,6] This activation is mediated by the renin–angiotensin system and numerous neurohumoral factors, including angiotensin II (Ang II) and transforming growth factor β1 (TGF-β1).[3,5] Ang II promotes the release of catecholamine and aldosterone, up-regulates the expression of TGF-β1 in fibroblasts, and is a strong promoting factor for cardiac fibrosis. It is also widely used *in vitro* to activate CFs or to induce cardiac fibrosis in animal models.[7] Markedly activated TGF-β1 interacts with renin–angiotensin system and mediates fibroblast activation and proliferation and is also the most effective fibrosis-promoting cytokine.[8,9] Together with Smad2/3, an essential component of the intracellular TGF-β1 signalling pathway, activation of the TGF-β1/Smad signalling pathway can facilitate fibrosis by stimulating collagen synthesis while inhibiting ECM degradation.[10] Although this signalling pathway has been extensively studied recently, effective preventive measures and treatments for cardiac fibrosis are still highly unsatisfactory.

Recent studies have shown that the intensity and duration of fibrosis-promoting signals are regulated by a cascade of multiple molecular interactions rather than an isolated pathway.[11,12] In our preliminary clinical study, we observed increased Slit2 expression levels and collagen deposition, accompanied by activation of TGF-β1 signalling, in the right atrial appendage of patients with valvular heart disease complicated by atrial fibrillation (AF), the most common form of arrhythmia. The Slit2 protein has been studied in lung and liver fibrosis, but its role in cardiac fibrosis is not established. Current lung research suggests that fibroblasts secrete Slit2, which inhibits the proliferation and differentiation of bleomycin-induced lung fibroblasts, and that exogenous Slit2 in the lung reduces fibrosis formation.[13] In contrast to Slit2's inhibitory function in the lung, another study demonstrated that in an animal model of liver fibrosis, the serum concentrations of Slit2 and Robo1 were significantly increased via a mechanism possibly related to the key TGF-β1–Smad pathway.[14] The Slit gene encodes glycoprotein ligands for the Robo family of immunoglobulin receptors; the Slit2–Robo1 signalling pathway has been reported to mediate some congenital heart diseases.[15] However, no reports have addressed the function of the Slit2–Robo1 signalling pathway in the adult animal heart. After reviewing the findings of previous clinical studies and reports, we speculated that the Slit2–Robo1 pathway plays a critical role in adult cardiac fibrosis, participating in the complex fibrosis-promoting pathway.

Material and methods

Human atrium tissue sample collection

A cohort of patients with clinically diagnosed valvular heart disease complicated by AF was evaluated based on their medical records and 12-lead electrocardiogram findings. Right atrial tissue samples were obtained from five patients during heart valve replacement surgery, and another five right atrial tissue samples were obtained from healthy heart donors without diagnosed AF. The tissue samples were obtained at the time of surgery and divided into two parts: one was immediately stored in liquid nitrogen for western blot analysis; the other was fixed with 4% paraformaldehyde for immunohistochemistry.

All clinical samples were obtained from The First Affiliated Hospital of Sun Yat-sen University, Guangzhou, China. The investigation complied with the principles of human tissue use outlined in the Declaration of Helsinki and was approved by the Human Ethics Committee of The First Affiliated Hospital of Sun Yat-sen University. Informed consent was obtained from all participants.

Animal model of transverse aortic constriction

Male C57BL mice (8–10 weeks old, 25–30 g, n = 30) were anaesthetised by intraperitoneal injection of xylazine (5 mg/kg) and ketamine (100 mg/kg) and were then subjected to transverse aortic constriction (TAC, n = 24) surgery or sham surgery (n = 6). The surgery was performed as follows[16]: under anaesthesia, a skin incision was made at the level of the second intercostal space, 2 mm to the left of the sternum. Then, the aortic arch was exposed by careful blunt dissection of the intercostal muscles, thymus, and other tissues. A 27G needle was placed at the telocentric end of the aortic arch and used to place a 7-0 silk ligature around the aorta. After removing the needle, we achieved a 0.4 mm diameter coarctation of the aorta. The sham surgery was the same procedure without aortic ligature.

The 24 animals that received TAC surgery were divided into four groups (n = 6). For 6 weeks after surgery, each group received different weekly intraperitoneal injections: (i) TAC + R5 group (40 mg/kg R5), (ii) TAC + SB431542 group (5 mg/kg SB431542), (iii) TAC + R5 + SB431542 group (40 mg/kg R5 + 5 mg/kg SB431542), and (iv) TAC group.[17,18] Mice in the TAC and sham groups were injected with saline at a volume equal to that saline used in the other groups.

Echocardiography

Tissue Doppler imaging (Vevo 2100 high-resolution ultrasound imaging system, VisualSonics, Toronto, ON, Canada)

was used to quantify heart function 6 weeks post surgery. A long-axis image was acquired at the cardiac apex. The left ventricular ejection fraction was calculated by a trace algorithm. A short-axis image was acquired at the level of the left ventricular papillary muscle adjacent to the sternum. The interventricular septal thickness at end-diastole and left ventricular posterior wall thickness were measured, and the left ventricular fractional shortening (FS (%) = [(LVIDd − LVIDs)/LVIDd × 100%]), left ventricular end-diastolic volume, and left ventricular stroke volume were calculated from the image. Ultrasound data were analysed in a double-blind manner by two ultrasound physicians. The averages of the two measurements were accepted as the final values.

Histology and immunohistochemistry

Body weights were measured 6 weeks post surgery. Then, the hearts from all mice were harvested, cleaned, and weighed. Sections were made along the short axis of the left ventricle. After fixation with 4% paraformaldehyde, Masson staining and haematoxylin–eosin (HE) staining were performed to evaluate the degree of myocardial hypertrophy and fibrosis. The remaining tissue was used for western blot analysis.

Masson staining was used to detect the expression of collagen and assess the degree of myocardial fibrosis. Slides of heart tissue were oxidized in 1% potassium permanganate solution for 5 min; bleached in oxalic acid for 1 min; stained in Celestine blue, Mayer's haematoxylin solution, and Ponceau S for 5 min each; and rinsed in 1% acetic acid water for 2 min. The slides were further differentiated in 1% phosphomolybdic acid for 5 min, stained with 1% light green or toluidine blue for 30 s, rinsed in 1% acetic acid water, and differentiated in 95% alcohol. After the aforementioned procedures, the slides were hydrated in absolute alcohol, cleared with xylene, and mounted with neutral resin. All slides were visualized with a light microscope (BX51, OLYMPUS, Tokyo, Japan). The fibrosis size was quantified using the ImageJ program.[19]

The HE staining process had several stages. Each section was first stained with haematoxylin buffer for 12 min, differentiated with 1% hydrochloric acid and alcohol for 20 s each, and subjected to bluing by incubation with 1% ammonia for 30 s. Each of the aforementioned steps was followed by washing with Scott blue staining solution for 1 min. Finally, the sections were stained with 0.5% eosin for 30 s and were then washed with tap water. The sections were dehydrated with ascending concentrations of ethanol (85%, 95%, and 100%). After staining was complete, all slides were sealed with neutral gum and evaluated with a light microscope.

Immunohistochemical staining was performed as follows: the sections were incubated in a humidified chamber at room temperature for 20–30 min, and goat serum was added as a blocking agent. Then, the primary antibody (30–50 μL) was added to the sections (TGF-β1, 1:100, Abcam, Cambridge, MA, USA; Slit2, 1:100, Proteintech, Rosemont, IL, USA; collagen I, 1:100, Abcam), which were then incubated at 4°C overnight. Then, a biotin-labelled secondary antibody (30–50 μL) was added to the sections at room temperature for 20 min. The sections were washed with phosphate-buffered saline, 3,3′-Diaminobenzid (DAB) colour development solution was added, and the sections were washed with distilled water. Finally, all sections were counterstained with haematoxylin for 1 min, differentiated using 0.1% hydrochloric acid alcohol for 5 s, and washed with running tap water for 20 min to allow bluing of haematoxylin in an alkaline environment. After staining was complete, the slides were evaluated under a light microscope.

Cardiac fibroblast isolation and cultivation

Cardiac fibroblasts were isolated from the ventricular tissues of male C57BL/6 mice (8–10 weeks old, 25–30 g, n = 5) obtained from the Experimental Animal Center, Sun Yat-sen University, Guangzhou, China. All procedures were performed in accordance with the Guide for the Care and Use of Laboratory Animals (NIH Publication No. 85-23, revised 1996). This study was approved by the Ethics Committee of The First Affiliated Hospital of Sun Yat-sen University. Mice were anaesthetised by intraperitoneal injection of a mixture of xylazine (5 mg/kg) and ketamine (100 mg/kg), and the ventricular tissues were harvested. Tissues were then washed with D-Hanks' solution to remove all blood components, minced into 1 mm^3 pieces, and digested by adding 0.25% trypsin at 37°C twice for 10 min each and 0.01% type I collagenase at 37°C for 120–180 min to obtain cell suspensions, which were filtered through a 40 μm nylon mesh and centrifuged at 180 g for 5 min. The cell pellets were resuspended and incubated in Dulbecco's Modified Eagle Medium (DMEM)/F12 (Gibco, USA) supplemented with 10% fetal bovine serum (Invitrogen, Carlsbad, CA, USA) and 1% penicillin/streptomycin (Gibco) at 37°C in a humidified atmosphere of 5% CO_2. Fibroblasts were identified by the differential adherence method. The adherent cells remaining after two differential adherence cultures of approximately 45 min to 1 h each were CFs.[20]

siRNA synthesis and transfection

The siRNA sequences targeting the mice *Slit2* gene (si-*Slit2*) and the mice *TGF-β1* gene (si-*TGF-β1*) and the scrambled siRNA sequence (si-Scramble) were designed and synthesized by RiboBio (Guangzhou, China). Passage 3 CFs were plated in a 6 well plate (1×10^5 cells/well) in 10% fetal bovine serum-containing medium and at 80% confluence were

starved by incubation in serum-free medium for 24 h. siRNAs (50 nM) were transfected into CFs with Lipofectamine™ RNAiMAX (Invitrogen) according to the manufacturer's protocol. Cells in the 1st–6th wells received the following treatments for 24: (i) 50 nM si-Scramble, (ii) 50 nM si-Scramble and 100 nM Ang II (Sigma, North St. Indianapolis, IN, USA), (iii) 50 nM si-*TGF-β1*, (iv) 50 nM si-*TGF-β1* and 100 nM Ang II, (v) 50 nM si-*Slit2*, and (vi) 50 nM si-*Slit2* and 100 nM Ang II. The second dose of Ang II, at the same concentration as the first dose, was added to the media after 12 h.

Immunofluorescence staining

Cardiac fibroblasts were divided into six groups as described in the Cardiac fibroblasts isolation and cultivation section and were then fixed with 4% paraformaldehyde for 20 min. CFs were incubated with rabbit polyclonal anti-collagen I (1:100, Abcam) and anti-Vimentin (1:100, CST, Beverly, MA, USA) primary antibodies overnight at 4°C and then with the DyLight 594 AffiniPure goat anti-rabbit IgG secondary antibody (1:100, EarthOx, Millbrae, CA, USA) for 1 h at room temperature. Nuclei were stained with 4′,6-diamidino-2-phenylindole (1 mg/mL; Solarbio, Tongzhou District, Beijing, China) for 5 min, and images were acquired using a Leica DMi8 (Buffalo Grove, IL, USA) inverted microscope (magnification: ×200).

Cell proliferation assay

Cardiac fibroblasts were seeded in 96 well plates (2×10^3 cells/well) overnight and were then divided into six groups as described previously in the Cardiac fibroblasts isolation and cultivation section. Each group comprised 6 wells and was treated as described in the siRNA synthesis and transfection section for 48 h. The degree of CF proliferation was measured using a Cell Counting Kit-8 (CCK-8; DOJINDO, Rockville, MA, USA), with CCK-8 solution (10 μL) added to each well. The plate was incubated for 4 h at 37°C. The absorbance at 450 nm was measured with a microplate reader (Thermo Scientific, Waltham, MA, USA).

RNA extraction and real-time PCR

RNA was extracted with a TaKaRa MiniBEST Universal RNA Extraction Kit (Takara, Kusatsu, Shiga, Japan) and reverse transcribed with PrimeScript™ RT Master Mix (Takara) according to the manufacturer's protocols. Real-time PCR was performed in a LightCycler 480 thermal cycler using SYBR Green PCR kits (Roche, Indianapolis, IN, USA) under the following conditions: (i) 95°C for 5 min and (ii) 34 cycles at 95°C for 10 s, 60°C for 20 s, and 72°C for 20s. Data were analysed with a Stratagene Mx3000p (Agilent Technologies, Santa Clara, CA, USA). GAPDH served as the internal control (for PCR primer sequences, see Supporting Information, Data S1).

Stimulation of cardiac fibroblasts using recombinant Slit2 and TGF-β1

Passage 3 CFs were seeded in 6 well plates and divided into the recombinant TGF-β1 (rTGF-β1), recombinant Slit2 (rSlit2), and control groups. At 60% confluence, the corresponding groups were treated with 10 mg/mL mouse rTGF-β1 (Biomart, Avenue Los Angeles, CA, USA), 100 ng/mL mouse rSlit2 (Cloud-Clone, Katy, TX, USA),[21,22] or no drug (control group). Cells were incubated for 24 h, and total protein was extracted for western blot analysis.

Western blot analysis

Homogenized myocardial tissue and CFs were lysed using radio immunoprecipitation assay buffer (CST) containing phenylmethanesulfonyl fluoride (Solarbio). Total protein (20 μg) was separated by 10% sodium dodecyl sulfate – polyacrylamide gel electrophoresis and transferred to polyvinylidene fluoride membranes (Millipore, Billerica, MA, USA). After blocking in 5% bovine serum albumin diluted with tris-buffered saline tween-20 at room temperature for 1 h, membranes were incubated overnight at 4°C with primary antibodies against TGF-β1 (1:1000, Abcam), Slit2 (1:1000, Proteintech), Robo1 (1:1000, Santa Cruz, Dallas, TX, USA), Smad2/3 (1:1000, CST), p-Smad2 (1:1000, CST), p-Smad3 (1:1000, CST), collagen I (1:1000, Abcam), PI3K (1:1000, CST), Akt (1:1000, CST), p-PI3K (1:1000, CST), p-Akt (1:1000, CST), and Periostin (1:1000, Abcam). Membranes were incubated with a horseradish peroxidase-conjugated goat anti-rabbit IgG secondary antibody (1:5000, CST) at room temperature for 1 h. Immunoreactive bands were visualized with ECL western blotting detection reagents (Millipore). Band densities were quantified by densitometry with Quantity One software (Bio-Rad Laboratories, Hercules, CA, USA). To ensure equal loading of samples, protein expression level was normalized to GAPDH.

Statistical analysis

Data are expressed as means ± standard deviations. Differences between discrete variables were evaluated by the χ^2 test; comparisons between two groups of continuous variables were evaluated by the Student's *t*-test; comparisons between more than two groups of continuous variables were evaluated by one-way ANOVA (SPSS Statistics 19.0, IBM, USA). Differences with $P < 0.05$ were considered statistically significant.

Results

Slit2–Robo1 signalling is activated in patients with cardiac fibrosis

The clinical data showed that the left and right atria of patients with valvular heart disease and AF were significantly larger than those of heart donors; in addition, the patients exhibited worsened cardiac function characterized by a significant decrease in ejection fraction (58.1 ± 7.7 vs. 69.6 ± 3.8%, $P = 0.008$) and higher N-terminal pro brain natriuretic peptide levels (964.3 ± 473.6 vs. 89.3 ± 50.6 pg/mL, $P = 0.0016$) than heart donors (*Table 1*). Masson staining of patient specimens revealed a more disordered arrangement and greater collagen deposition than observed in donor specimens, which did not exhibit substantial collagen deposition. HE staining showed that patients' cardiomyocytes were significantly more disordered and hypertrophied than donors' (*Figure 1A*).

Immunocytochemistry revealed significantly increased expression levels of collagen I, TGF-β1, and Slit2 in the right atrial appendage of patients with valvular heart disease complicated by AF (*Figure 1B*). Western blot analysis of the right atrial myocardium suggested that the protein expression of TGF-β1 and collagen I was significantly up-regulated in the patient cohort (*Figure 1C, D–G*). Similarly, Slit2–Robo1 expression was significantly increased in heart patients, indicating the Slit2–Robo1 signalling pathway associated with cardiac fibrosis (*Figure 1C, D–G*).

Cardiac function and remodelling

Tissue Doppler imaging revealed that TAC mice had enlarged hearts, thickened myocardia, decreased systolic function, and increased heart weight/body weight ratios compared with sham mice. Treatment with R5 (the Robo1 antagonist) or SB431542 (the TGF-β1 antagonist) partially reversed the effect of TAC surgery (*Figure 2A–E*, *Table 2*). Masson staining showed a significant proliferation of the fibrous myocardial connective tissue in the TAC group compared with the sham group (*Figure 2F–G*). In the sham group, the Slit2, Robo1, and collagen I expression levels were low, and the TGF-β1 level was high. The Slit2, Robo1, collagen I, and TGF-β1 expression levels were increased in the TAC group (*Figure 2H–L*), suggesting that TAC surgery can lead to cardiac fibrosis in mice and up-regulation of Slit2, Robo1, and TGF-β1 expression. In the SB431542 and R5 + SB431542 groups, the collagen I and TGF-β1 expression levels were lower than those of the TAC group but higher than those of the sham group, suggesting that R5 and SB431542 can alleviate the effects of TAC. The TAC + R5, TAC + SB431542, and TAC + R5 + SB431542 groups had lower Robo1 expression levels than the TAC group, although the difference was statistically insignificant, and significantly higher Robo1 expression levels than the sham group. The R5 group had the highest Slit2 expression level, which was significantly higher than that in the TAC group ($P < 0.05$). Further experiments might be needed to address this observation.

Table 1 Clinical data of patients with valvular heart disease complicated by AF and healthy heart donors

	AF patients	Healthy donors	*P*-value
Age (years)	51.8 ± 8.9	30.8 ± 7.3	0.007
Gender			
Female	3	0	0.083
Male	2	5	0.257
Diagnosis			
MI	4	0	<0.001
MS	5	0	<0.001
TI	5	0	<0.001
AF	5	0	<0.001
Atrial diameter (mm)			
RA	67.8 ± 9.8	33.8 ± 1.8	<0.001
LA	68.2 ± 25.7	34.6 ± 2.9	0.014
LVEF (%)	58.1 ± 7.7	69.6 ± 3.8	0.008
NT-proBNP (pg/mL)	964.3 ± 473.6	89.3 ± 50.6	0.0016

AF, atrial fibrillation; LA, left atrial; LVEF, left ventricular ejection fraction; MI, mitral valve insufficiency; MS, mitral valve stenosis; NT-proBNP, N-terminal portion of pro-BNP; RA, right atrial; TI, tricuspid valve insufficiency.

Slit2 knockdown inhibits Ang II-induced collagen I production and cardiac fibroblasts proliferation

The positive control group was treated with Ang II, a common activator of CFs, to establish an *in vitro* cellular model of cardiac fibrosis.[10] The immunofluorescence staining results showed that si-*Slit2* and si-*TGF-β1* significantly inhibited Ang II-induced collagen I and Vimentin overexpression, which was obvious in the si-Scramble group (*Figure 3A–B*). Separate measurements of the Slit2 ligand subtypes Robo1–4 in CFs demonstrated that the Robo1 expression level was significantly higher than that of Robo2 ($P < 0.05$); however, almost no expression of Robo3 or Robo4 was detected (*Figure 3C*). The CCK-8 assay results showed that siRNA transfection significantly inhibited Ang II-induced proliferation of CFs (*Figure 3D*). The real-time PCR results confirmed that Ang II up-regulated the expression of *Slit2* and *TGF-β1* mRNA. However, this effect was dramatically inhibited by both si-*Slit2* and si-*TGF-β1* (*Figure 3E–F*). si-*Slit2* down-regulated *TGF-β1* mRNA expression, but si-*TGF-β1* did not significantly impact *Slit2* mRNA expression (*Figure 3E–F*).

The Slit2–Robo1 signalling pathway is involved in cardiac fibrosis

Angiotensin II stimulation increased the Slit2, Robo1, TGF-β1, and collagen I protein expression levels in CFs compared with

Figure 1 Slit2–Robo1 signalling is activated in patients with valvular heart disease complicated by atrial fibrillation (AF). (A) Masson and haematoxylin–eosin (HE) staining of the right atrial myocardium. In the Masson-stained sections, collagen fibres are stained blue, muscle fibres and erythrocytes red, and nuclei bluish-brown. Substantial collagen deposition was identified in the right atrial tissue of patients, and no significant collagen deposition was observed in that of healthy donors. HE staining indicated disorder and significant hypertrophy of myocardial cells. (B) Immunocytochemistry of collagen I, TGF-β1, and Slit2 in the right atrial myocardium. The expression levels of collagen I, TGF-β1, and Slit2 were significantly higher in cardiac fibroblasts of patients with valvular heart disease complicated by AF than in those of healthy donors. (C) Western blot analysis of Slit2, Robo1, TGF-β1, and collagen I expression levels. (D–G) Bar chart of the expression ratios from western blotting normalized to GAPDH. Data are presented as the means ± standard deviations, $n = 5$. $^*P < 0.05$ vs. the healthy donor group.

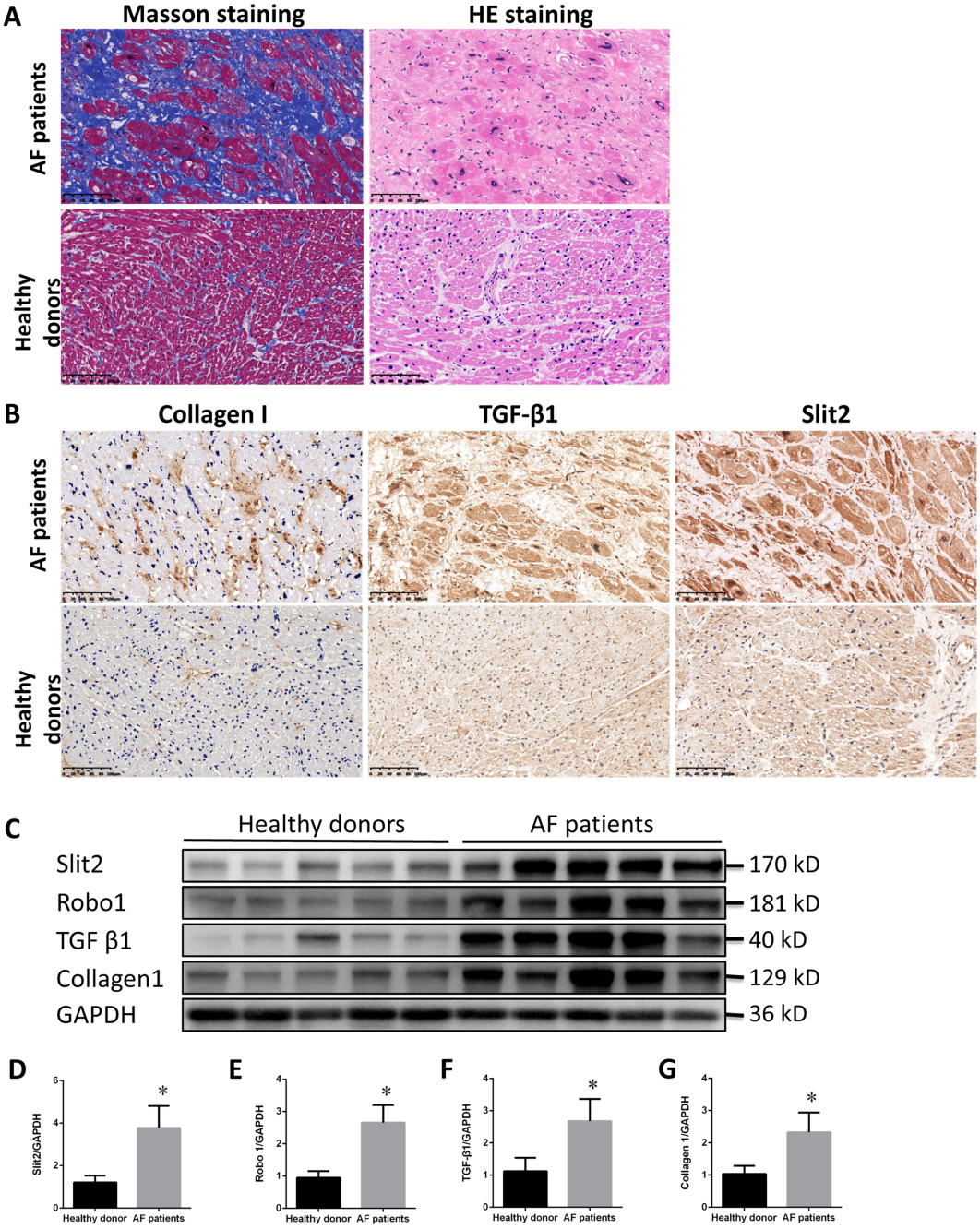

Figure 2 Cardiac remodelling and function in the mouse model of transverse aortic constriction (TAC). (A) Echocardiographic short-axis images and cardiac function measurements of all groups. (B–E) Quantification of cardiac function measurements and heart weight/body weight in all mouse groups. LVPW, left ventricular posterior wall thickness; LVSD, left ventricular end-systolic diameter; LVDV, left ventricular end-diastolic volume; IVSD, interventricular septal thickness at end-diastole; LVSV, left ventricular stroke volume; LVFS, left ventricular fractional shortening; LVEF, left ventricular ejection fraction. (F) Masson staining of mouse left ventricles. Collagen fibres are stained blue, muscle fibres and erythrocytes red, and nuclei bluish-brown (×200). (G) Masson staining showed that the collagen content in the muscle bundles of myocardial tissue from the TAC and the drug-treated groups was significantly increased compared with that in the sham group. (H) Representative western blot of left ventricle tissue. (I–L) Quantitative analysis of Slit2, Robo1, TGF-β1, Smad2/3, and collagen I expressions. GAPDH was used as the internal control. Data are presented as the means ± standard deviations, $n = 6$. $^{*}P < 0.05$ vs. the sham control group; $\#P < 0.05$ vs. the TAC control group.

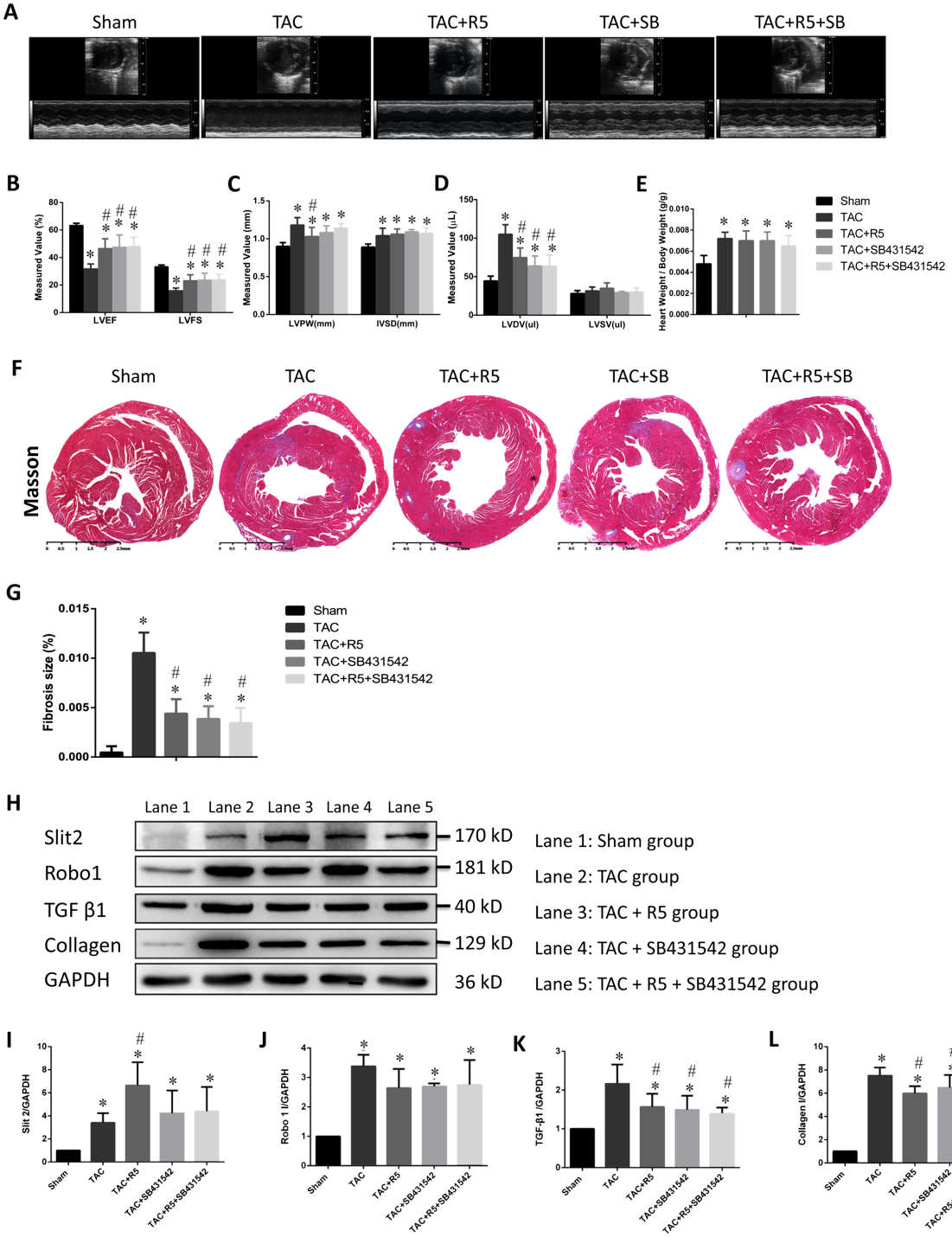

DOI: 10.1002/ehf2.13095

Table 2 Echocardiography data in the mouse model of TAC

Parameter	Sham	TAC	TAC + R5	TAC + SB431542	TAC + R5 + SB431542
LVPW (mm)	0.90 ± 0.05	1.18 ± 0.10*	1.03 ± 0.12*, **	1.08 ± 0.09*	1.14 ± 0.06*
IVSD (mm)	0.89 ± 0.04	1.04 ± 0.10*	1.06 ± 0.07*	1.09 ± 0.03*	1.07 ± 0.07*
LVDV (μL)	44.28 ± 6.40	104.80 ± 12.57*, **	74.71 ± 12.46*, **	63.82 ± 13.00*, **	63.58 ± 14.40*, **
LVSV (μL)	28.00 ± 3.94	31.42 ± 5.20	34.82 ± 7.10	29.28 ± 1.66	30.07 ± 5.53
EF (%)	63.27 ± 1.59	31.80 ± 3.50*, **	46.66 ± 6.98*, **	47.58 ± 8.79*, **	48.10 ± 6.67*, **
FS (%)	33.36 ± 1.18	15.97 ± 1.83*, **	23.19 ± 4.22*, **	23.66 ± 4.98*, **	23.89 ± 3.94*, **

EF, ejection fraction; FS, fractional shortening; IVSD, interventricular septal thickness at end-diastole; LVDV, left ventricular end-diastolic volume; LVPW, left ventricular posterior wall thickness; LVSV, left ventricular stroke volume; TAC, transverse aortic constriction.
*$P < 0.05$ vs. the sham control group.
**$P < 0.05$ vs. the TAC control group.

those in the si-Scramble group, which served as the negative control group and baseline for western blot analysis (*Figure 4A–E*). Transfection of si-*Slit2* or si-*TGF-β1* reduced the protein expression levels of Slit2, Robo1, TGF-β1, and collagen I in CFs to very low levels; re-addition of Ang II after the first transfection only partially restored the expression levels (*Figure 4A–E*). Previous studies revealed that Ang II regulates cardiac fibrosis via the TGF-β1–Smad signalling pathway.[9,10] In this study, siRNA transfection significantly inhibited Smad2 phosphorylation, but neither si-*Slit2* nor si-*TGF-β1* impacted Smad3 phosphorylation (*Figure 4F–H*).

The PI3K/Akt pathway is involved in regulating cardiac fibroblast activity via Slit2–Robo1 signalling

The PI3K/Akt signalling pathway plays an important role in the modulation of cardiac fibrosis.[23] We performed western blotting to determine the phosphorylation levels of PI3K and Akt and found that Ang II significantly increased the phosphorylation of PI3K and Akt, but this effect was effectively inhibited by transfection with si-*TGF-β1* or si-*Slit2* (*Figure 5A–E*). However, the levels of total PI3K and Akt did not differ significantly (*Figure 5A–E*).

Recombinant Slit2 activates the Smad signalling pathway and up-regulates Periostin expression in cardiac fibroblasts

After treatment with rTGF-β1, the Slit2 expression level in CFs increased non-significantly (*Figure 6A, E*). However, the TGF-β 1 expression level in CFs was increased significantly by rSlit2 (*Figure 6B, F*). Both rSlit2 and rTGF-β1 promoted Smad2 and Smad3 phosphorylation and significantly up-regulated Periostin, Robo1, and collagen I expressions (*Figure 6C–D, G–K*).

Discussion

The Slit2–Robo1 signalling pathway has been reported to participate in many physiological processes, including axon guidance, neuronal migration, and leucocyte chemotaxis.[24–27] Previous studies have shown that activation of Slit2–Robo1 signalling promotes liver fibrosis.[14] Our clinical research suggested that Slit2–Robo1 signalling is also activated in cardiac fibrosis, suggesting that it may play a role in cardiac fibrosis.

Atrial fibrillation, the most common clinical arrhythmia, correlates with poor cardiac electrical and structural remodelling.[28] The consequence of AF includes structural remodelling of the atrium and ventricle, which reciprocally promotes AF development.[29] Previous studies have reported that TGF-β1 may play an important role in AF occurrence and progression.[24,27] TGF-β1 is the most potent profibrotic cytokine and is a key mediator of fibroblast activation and fibrosis in heart diseases.[30] Increasing expression of TGF-β1 in atrial tissue is associated with increased susceptibility to atrial fibrosis and AF.[31] Activation of the TGF-β1/α-SMA/collagen I profibrotic pathway by Galectin-3 in fibroblasts contributes actively to atrial fibrosis in both patients and experimental AF models.[32] Therefore, we used TGF-β1 and collagen I as control molecules to observe the degree of cardiac fibrosis/CF activation in clinical specimens and CFs *in vitro*.

The expression levels of TGF-β1 and collagen I, as well as those of Slit2 and Robo1, were significantly higher in the right atrial appendages of AF patients than in those of healthy donors, indicating fibrosis in the right atrial appendage of patients. The results indicating Slit2–Robo1 pathway activation also suggested the correlation of this pathway with cardiac fibrosis. TAC leads to cardiac hypertrophy and cardiac fibrosis in mice.[16] The reduced expression of TGF-β1 and collagen I in the SB431542 and R5 + SB431542 groups and alleviation of myocardial remodelling and fibrosis suggest that suppressing the Robo1 and/or the TGF-β1–Smad signalling pathway can lead to suppression of cardiac fibrosis. The high expression level of Ang II in atrial tissue of patients with valvular heart disease can significantly up-regulate TGF-β1 expression and promote cardiac fibrosis.[33,34] Here, adding Ang II to CF

Figure 3 The effect of siRNA and angiotensin II (Ang II) on cardiac fibroblasts (CFs). CFs were transfected with si-*TGF-β1* and si-*Slit2* and then treated with or without Ang II for 24 h in serum-free medium. (A) Immunofluorescence staining of collagen I; (B) immunofluorescence staining of Vimentin. Collagen I is stained red. Vimentin is stained green. Scale bar = 75 μm (images acquired at ×200). (C) Expression levels of the four Robo receptors, as determined by quantitative PCR. The Robo1 expression level was significantly higher than that of Robo2, and those of Robo3 and Robo4 were negligible. (D) Cell Counting Kit-8 cell proliferation assay. Compared with the si-Scramble group, the si-*TGF-β1* and si-*Slit2* groups exhibited significantly inhibited CF proliferation; Ang II only partially restored CF proliferation. (E–F) Bar chart showing the ratio of the *TGF-β1* and *Slit2* mRNA expression levels in CFs as determined by quantitative PCR and normalized to GAPDH. Data are presented as the means ± standard deviations, $n = 5$. $^{*}P < 0.05$ vs. the si-Scramble group without Ang II; $^{\#}P < 0.05$ vs. the si-Scramble + Ang II group.

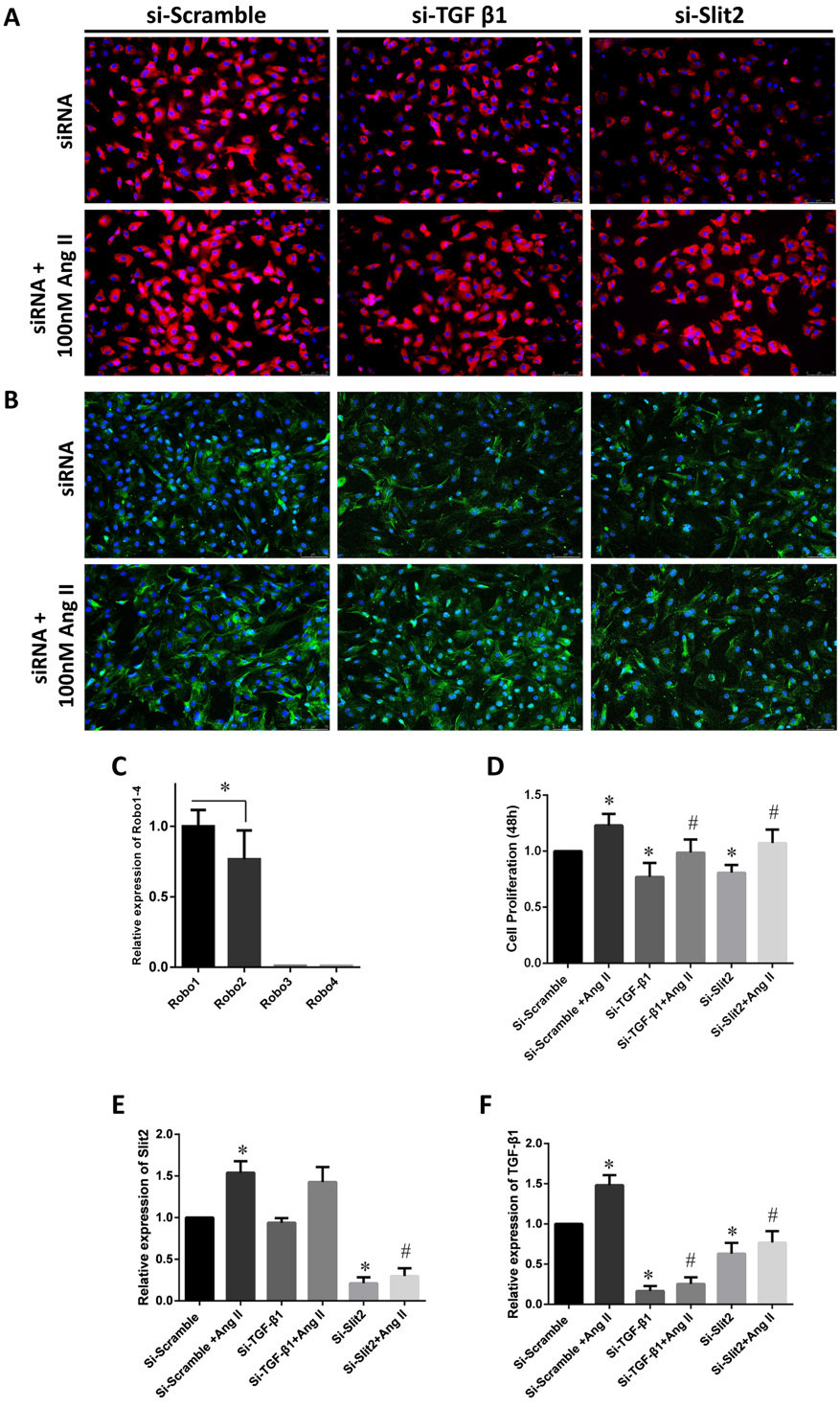

DOI: 10.1002/ehf2.13095

Figure 4 The Slit2–Robo1 signalling pathway is involved in cardiac fibrosis. (A) si-*Slit2* siRNA and si-*TGF-β1* suppressed collagen I expression in cardiac fibroblasts. Cardiac fibroblasts were transfected with si-*TGF-β1* or si-*Slit2* and then treated with or without Ang II for 24 h in serum-free medium. (B–E) Bar chart showing the ratio of total Slit2, Robo1, TGF-β1, and collagen I protein expression levels normalized to GAPDH. (F) Western blot analysis of p-Smad2, p-Smad3, and Smad2/3 expressions after treatment with siRNAs or siRNAs + Ang II. (G–H) Bar charts showing the expression ratios of related proteins normalized to GAPDH. Data are presented as the means ± standard deviations, $n = 5$. *$P < 0.05$ vs. the corresponding control group without Ang II; #$P < 0.05$ vs. the si-Scramble + Ang II group.

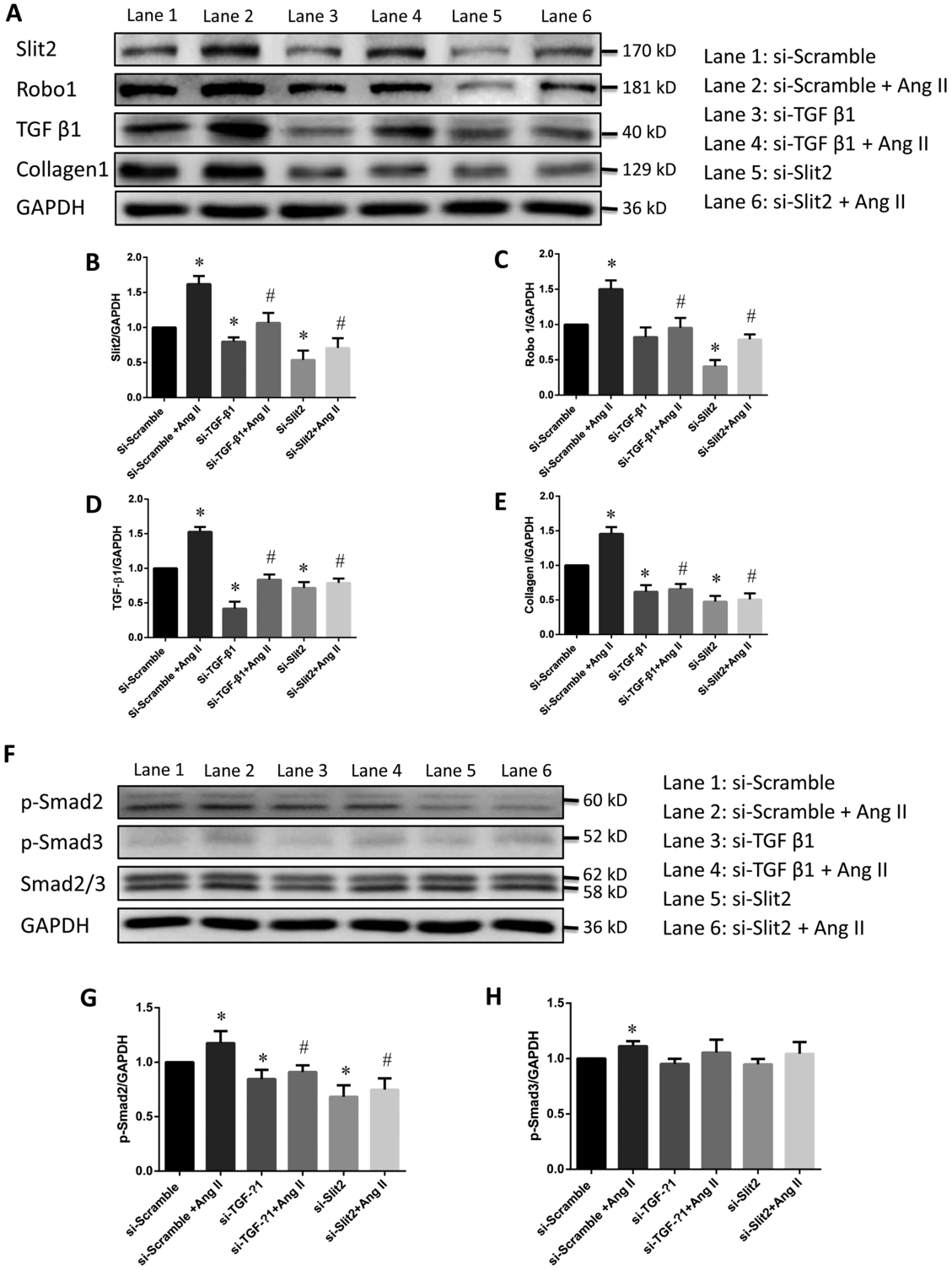

Figure 5 The PI3K/Akt pathway is involved in the regulation of Slit2–Robo1 signalling in cardiac fibroblasts. (A) Western blot results for PI3K, p-PI3K, Akt, and p-Akt. (B–E) Bar charts of the expression ratios of related proteins normalized to GAPDH for each group. Data are presented as the means ± standard deviations, $n = 5$. *$P < 0.05$ vs. the corresponding control group without Ang II; #$P < 0.05$ vs. the si-Scramble + Ang II group.

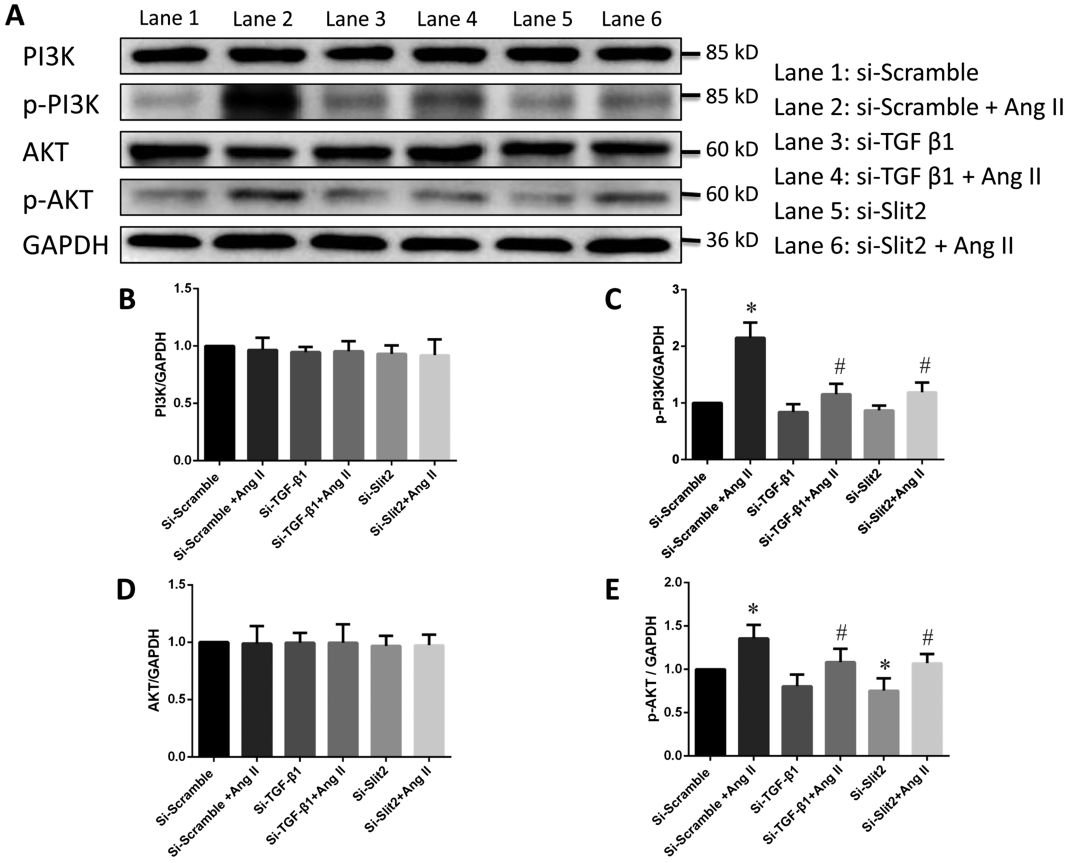

culture medium led to significant increases in TGF-β1, Smad2/3, collagen I, Slit2, and Robo1 expressions. Transfection of si-*Slit2* inhibited TGF-β1, Smad2/3, Robo1, and collagen I expressions and effectively inhibited the effects of Ang II on TGF-β1, Smad2/3, and collagen I expressions. Both si-*Slit2* and si-*TGF-β1* significantly inhibited Ang II-induced collagen I expression. These results strongly suggest that Slit2–Robo1 signalling is involved in cardiac fibrosis and is closely related to the Ang II/TGF-β1–Smad2/3 pathway.

Previous studies have revealed that aspects of profibrotic processes, especially the regulation of the profibrotic signal intensity and duration, are controlled by a network cascade of multiple molecular interactions rather than an isolated pathway.[35,36] Our experiments reconfirmed that the cardiac fibrosis process relies on complex molecular regulatory networks. Interestingly, the effect of si-*Slit2* transfection on *TGF-β1* expression in CFs was equivalent to that of direct transfection of si-*TGF-β1*. The effect of *Slit2* knockdown on the p-Smad2 and collagen I levels was stronger than that of *TGF-β1* knockdown. These results suggest that Slit2 is located upstream of TGF-β1 in the Ang II-induced cardiac fibrosis molecular network. However, *TGF-β1* knockdown also slightly down-regulated *Slit2* expression, but the effect was less significant, indicating the possible existence of a feedback mechanism between Slit2 and TGF-β1 network. Independent treatment of CFs with rSlit2 and rTGF-β1 revealed that rSlit2 significantly promotes TGF-β1 synthesis, although rTGF-β1 did not significantly affect Slit2 synthesis. This result indicated that Slit2 is upstream of TGF-β1 in the CF activation pathway.

Here, Ang II treatment activated the PI3K/Akt pathway in CFs, whereas *Slit2* or *TGF-β1* knockdown inhibited PI3K/Akt signalling. The PI3K/Akt signalling pathway plays an important role in the regulation of cardiac fibrosis.[23] The PI3K inhibitor NVP-BEZ235 can block BMI1-induced cardiac fibrosis.[37] Fusaric acid protects against HF by preventing cardiac fibrosis via modulation of the TGF-β1–Smad and PI3K/Akt signalling pathways.[38] Chang *et al*. reported that the PI3K/Akt pathway promotes liver fibrosis after activation of Slit2–Robo1 signalling.[14] rSlit2 promotes liver fibrosis by activating the PI3K/Akt signalling pathway, whereas addition of the PI3K/Akt antagonist LY294002 inhibits this effect.[22] These findings imply that the Slit2–Robo1, TGF-β1–Smad, and PI3K/Akt

Figure 6 Recombinant Slit2 (rSlit2) promotes Periostin expression and activates Smad signalling. (A) Recombinant TGF-β1 (rTGF-β1) promoted Slit2 expression. (B) rSlit2 significantly promoted TGF-β1 expression. (C–D) Recombinant proteins promoted Periostin, Robo1, and collagen I expressions and Smad2/3 phosphorylation. (E–K) Bar charts of the expression ratios of related proteins normalized to GAPDH for each group. Data are presented as the means ± standard deviations, $n = 5$. *$P < 0.05$ vs. the corresponding control group.

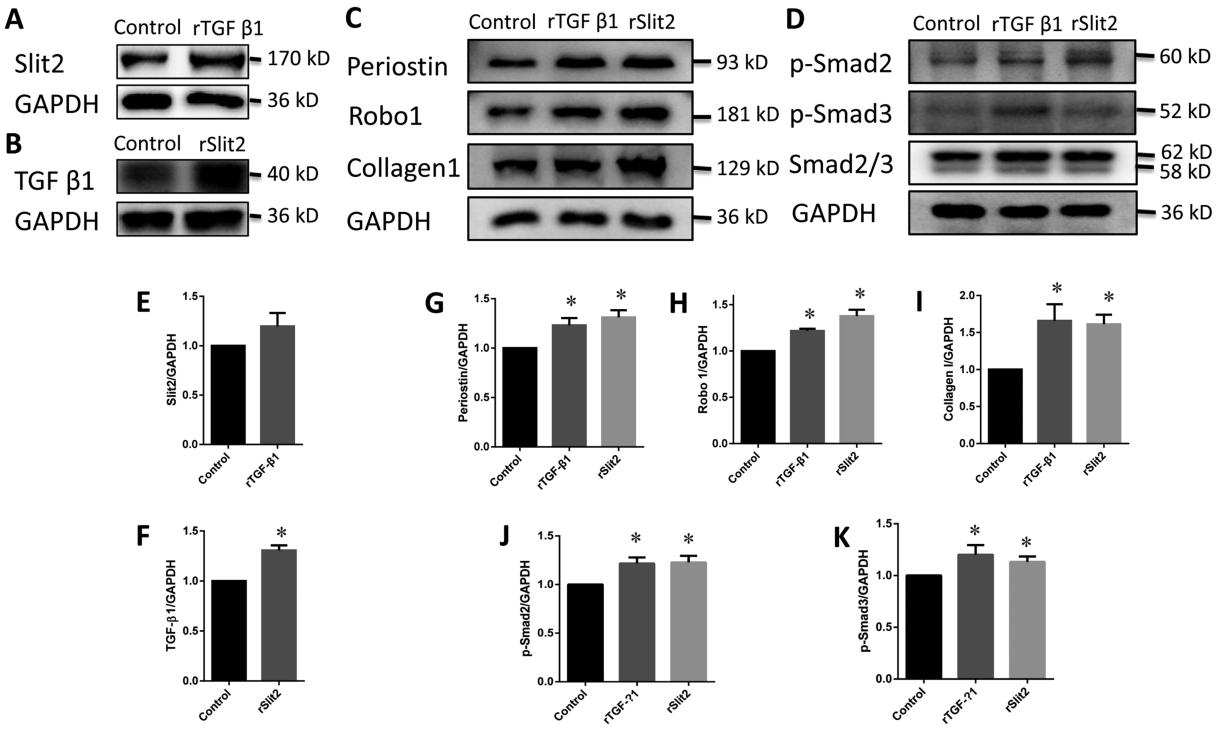

pathways might be involved in fibrosis regulation. Our results suggest that the PI3K/Akt signalling pathway is involved with the Slit2–Robo1 and TGF-β1–Smad pathways in cardiac fibrosis. However, the specific molecular mechanisms remain to be further studied.

As a non-structural component of the ECM, Periostin cooperates with TGF-β signalling, mediates cell–matrix signal transduction, and plays an important role in fibrosis in both the heart and other organs.[39,40] In healthy tissue, the expression of Periostin is low, but in damaged hearts or blood vessels, cardiac myofibroblasts and vascular smooth muscle cells are activated, leading to synthesis and release of Periostin, which mediates the reconstruction of cardiac interstitial tissue.[39,41] Our study revealed that both rSlit2 and rTGF-β1 can promote Smad2/3 phosphorylation and significantly up-regulate collagen I, Robo1, and Periostin synthesis. These results demonstrated that Periostin participates in the cardiac fibrosis pathways mediated by Slit2–Robo1 signalling.

In summary, our results showed that Slit2–Robo1 signalling is activated in fibrotic heart tissues, acting as part of the cardiac fibrosis-promoting component. The exact molecular mechanism underlying the role of the Slit2–Robo1 pathway in cardiac fibrosis, especially its relationship with TGF-β1 and Periostin, needs further exploration. Slit2 exerts its profibrotic effects at least partially via activation of TGF-β1–Smad, PI3K/Akt, and Periostin signalling. Hence, blockade of Slit2–Robo1 signalling may offer a novel therapeutic approach for preventing cardiac fibrosis.

Conflict of interest

The authors declare that they have no conflict of interest.

Funding

This work was supported by the Science and Technology Planning Project of Guangdong Province (2014A020215007 and 2015B010125001) and the Science and Technology Program of Guangzhou City (201803010077).

Author contributions

Y.L., Z.Y., J.Y., and X.X. were involved in conception and design, performance of experiments, data analysis and

interpretation and manuscript writing; X.X., J.Y., and C.L. were involved in the development of methodology; X.D. and Q.S. were involved in the data acquisition; Y.T. was involved in the histology and immunohistochemistry assay; Y.L., J.Y., and S.Y. were involved in study supervision and final approval of the manuscript.

Supporting information

Additional supporting information may be found online in the Supporting Information section at the end of the article.

Data S1. The PCR primer sequences.

References

1. Tomasoni D, Adamo M, Lombardi CM, Metra M. Highlights in heart failure. *ESC Heart Fail* 2019; **6**: 1105–1127.
2. Guo Y, Gupte M, Umbarkar P, Singh AP, Sui JY, Force T, Lal H. Entanglement of GSK-3β, β-catenin and TGF-β1 signaling network to regulate myocardial fibrosis. *J Mol Cell Cardiol* 2017; **110**: 109–120.
3. Meagher P, Adam M, Connelly K. It's not all about the cardiomyocyte: fibroblasts, empagliflozin, and cardiac remodelling. *Can J Cardiol* 2020; **36**: 464–466.
4. Souders CA, Bowers SL, Baudino TA. Cardiac fibroblast: the renaissance cell. *Circ Res* 2009; **105**: 1164–1176.
5. Gourdie RG, Dimmeler S, Kohl P. Novel therapeutic strategies targeting fibroblasts and fibrosis in heart disease. *Nat Rev Drug Discov* 2016; **15**: 620–638.
6. Landry N, Kavosh MS, Filomeno KL, Rattan SG, Czubryt MP, Dixon IMC. Ski drives an acute increase in MMP-9 gene expression and release in primary cardiac myofibroblasts. *Physiol Rep* 2018; **6**: e13897.
7. Rai V, Sharma P, Agrawal S, Agrawal DK. Relevance of mouse models of cardiac fibrosis and hypertrophy in cardiac research. *Mol Cell Biochem* 2017; **424**: 123–145.
8. Arribillaga L, Dotor J, Basagoiti M, Riezu-Boj JI, Borrás-Cuesta F, Lasarte JJ, Sarobe P, Cornet ME, Feijoó E. Therapeutic effect of a peptide inhibitor of TGF-β on pulmonary fibrosis. *Cytokine* 2011; **53**: 327–333.
9. Zhu Y, Gu J, Zhu T, Jin C, Hu X, Wang X. Crosstalk between Smad2/3 and specific isoforms of ERK in TGF-β1-induced TIMP-3 expression in rat chondrocytes. *J Cell Mol Med* 2017; **21**: 1781–1790.
10. Zhang Y, Huang XR, Wei LH, Chung AC, Yu CM, Lan HY. miR-29b as a therapeutic agent for angiotensin II-induced cardiac fibrosis by targeting TGF-β/Smad3 signaling. *Mol Ther* 2014; **22**: 974–985.
11. Lal H, Ahmad F, Zhou J, Yu JE, Vagnozzi RJ, Guo Y, Yu D, Tsai EJ, Woodgett J, Gao E, Force T. Cardiac fibroblast glycogen synthase kinase-3β regulates ventricular remodeling and dysfunction in ischemic heart. *Circulation* 2014; **130**: 419–430.
12. Woodall MC, Woodall BP, Gao E, Yuan A, Koch WJ. Cardiac fibroblast GRK2 deletion enhances contractility and remodeling following ischemia/reperfusion injury. *Circ Res* 2016; **119**: 1116–1127.
13. Pilling D, Zheng Z, Vakil V, Gomer RH. Fibroblasts secrete Slit2 to inhibit fibrocyte differentiation and fibrosis. *Proc Natl Acad Sci USA* 2014; **111**: 18291–18296.
14. Chang J, Lan T, Li C, Ji X, Zheng L, Gou H, Ou Y, Wu T, Qi C, Zhang Q, Li J, Gu Q, Wen D, Cao L, Qiao L, Ding Y, Wang L. Activation of Slit2–Robo1 signaling promotes liver fibrosis. *J Hepatol* 2015; **63**: 1413–1420.
15. Zhao J, Mommersteeg MTM. Slit–Robo signalling in heart development. *Cardiovasc Res* 2018; **114**: 794–804.
16. Song S, Liu L, Yu Y, Zhang R, Li Y, Cao W, Xiao Y, Fang G, Li Z, Wang X, Wang Q, Zhao X, Chen L, Wang Y, Wang Q. Inhibition of BRD4 attenuates transverse aortic constriction- and TGF-β-induced endothelial-mesenchymal transition and cardiac fibrosis. *J Mol Cell Cardiol* 2019; **127**: 83–96.
17. Yao Y, Zhou Z, Li L, Li J, Huang L, Li J, Qi C, Zheng L, Wang L, Zhang QQ. Activation of Slit2/Robo1 signaling promotes tumor metastasis in colorectal carcinoma through activation of the TGF-β/Smads pathway. *Cell* 2019; **8**: 635.
18. Zankov DP, Shimizu A, Tanaka-Okamoto M, Miyoshi J, Ogita H. Protective effects of intercalated disk protein afadin on chronic pressure overload-induced myocardial damage. *Sci Rep* 2017; **7**: 39335.
19. Kim HB, Hong YJ, Park HJ, Ahn Y, Jeong MH. Effects of ivabradine on left ventricular systolic function and cardiac fibrosis in rat myocardial ischemia-reperfusion model. *Chonnam Med J* 2018; **54**: 167–172.
20. Kaneko T, Nomura F, Yasuda K. On-chip constructive cell-network study (I): contribution of cardiac fibroblasts to cardiomyocyte beating synchronization and community effect. *J Nanobiotechnol* 2011; **9**: 21.
21. Tao L, Bei Y, Chen P, Lei Z, Fu S, Zhang H, Xu J, Che L, Chen X, Sluijter JP, Das S, Cretoiu D, Xu B, Zhong J, Xiao J, Li X. Crucial role of miR-433 in regulating cardiac fibrosis. *Theranostics* 2016; **6**: 2068–2083.
22. Zeng Z, Wu Y, Cao Y, Yuan Z, Zhang Y, Zhang DY, Hasegawa D, Friedman SL, Guo J. Slit2–Robo2 signaling modulates the fibrogenic activity and migration of hepatic stellate cells. *Life Sci* 2018; **203**: 39–47.
23. Chou CH, Hung CS, Liao CW, Wei LH, Chen CW, Shun CT, Wen WF, Wan CH, Wu XM, Chang YY, Wu VC, Wu KD, Lin YH, TAIPAI Study Group. IL-6 trans-signalling contributes to aldosterone-induced cardiac fibrosis. *Cardiovasc Res* 2018; **114**: 690–702.
24. Dallol A, Morton D, Maher ER, Latif F. SLIT2 axon guidance molecule is frequently inactivated in colorectal cancer and suppresses growth of colorectal carcinoma cells. *Cancer Res* 2003; **63**: 1054–1058.
25. Gu JJ, Gao GZ, Zhang SM. miR-218 inhibits the migration and invasion of glioma U87 cells through the Slit2–Robo1 pathway. *Oncol Lett* 2015; **9**: 1561–1566.
26. Mertsch S, Schmitz N, Jeibmann A, Geng JG, Paulus W, Senner V. Slit2 involvement in glioma cell migration is mediated by Robo1 receptor. *J Neurooncol* 2008; **87**: 1–7.
27. Plachez C, Andrews W, Liapi A, Knoell B, Drescher U, Mankoo B, Zhe L, Mambetisaeva E, Annan A, Bannister L, Parnavelas JG, Richards LJ, Sundaresan V. Robos are required for the correct targeting of retinal ganglion cell axons in the visual pathway of the brain. *Mol Cell Neurosci* 2008; **37**: 719–730.
28. Wijffels MC, Kirchhof CJ, Dorland R, Allessie MA. Atrial fibrillation begets atrial fibrillation. A study in awake chronically instrumented goats. *Circulation* 1995; **92**: 1954–1968.
29. Platonov PG, Mitrofanova LB, Orshanskaya V, Ho SY. Structural abnormalities in atrial walls are associated with presence and persistency of atrial fibrillation but not with age. *J Am Coll Cardiol* 2011; **58**: 2225–2232.
30. Khalil H, Kanisicak O, Prasad V, Correll RN, Fu X, Schips T, Vagnozzi RJ, Liu R, Huynh T, Lee SJ, Karch J, Molkentin JD. Fibroblast-specific TGF-β-Smad2/3

signaling underlies cardiac fibrosis. *J Clin Invest* 2017; **127**: 3770–3783.
31. Qiu H, Wu H, Ma J, Cao H, Huang L, Qiu W, Peng Y, Ding C. DL-3-*n*-Butylphthalide reduces atrial fibrillation susceptibility by inhibiting atrial structural remodeling in rats with heart failure. *Naunyn Schmiedebergs Arch Pharmacol* 2018; **391**: 323–334.
32. Shen H, Wang J, Min J, Xi W, Gao Y, Yin L, Yu Y, Liu K, Xiao J, Zhang YF, Wang ZN. Activation of TGF-β1/α-SMA/Col I profibrotic pathway in fibroblasts by galectin-3 contributes to atrial fibrosis in experimental models and patients. *Cell Physiol Biochem* 2018; **47**: 851–863.
33. Leask A. Potential therapeutic targets for cardiac fibrosis: TGFbeta, angiotensin, endothelin, CCN2, and PDGF, partners in fibroblast activation. *Circ Res* 2010; **106**: 1675–1680.
34. Nagata S, Varagic J, Kon ND, Wang H, Groban L, Simington SW, Ahmad S, Dell'Italia LJ, VonCannon JL, Deal D, Ferrario CM. Differential expression of the angiotensin-(1-12)/chymase axis in human atrial tissue. *Ther Adv Cardiovasc Dis* 2015; **9**: 168–180.
35. Davis J, Salomonis N, Ghearing N, Lin SC, Kwong JQ, Mohan A, Swanson MS, Molkentin JD. MBNL1-mediated regulation of differentiation RNAs promotes myofibroblast transformation and the fibrotic response. *Nat Commun* 2015; **6**: 10084.
36. Molkentin JD, Bugg D, Ghearing N, Dorn LE, Kim P, Sargent MA, Gunaje J, Otsu K, Davis J. Fibroblast-specific genetic manipulation of p38 MAPK in vivo reveals its central regulatory role in fibrosis. *Circulation* 2017; **136**: 549–561.
37. Yang W, Wu Z, Yang K, Han Y, Chen Y, Zhao W, Huang F, Jin Y, Jin W. BMI1 promotes cardiac fibrosis in ischemia-induced heart failure via the PTEN–PI3K/AKT–mTOR signaling pathway. *Am J Physiol Heart Circ Physiol* 2019; **316**: H61–H69.
38. Li X, Zhang ZL, Wang HF. Fusaric acid (FA) protects heart failure induced by isoproterenol (ISP) in mice through fibrosis prevention via TGF-β1–Smads and PI3K/AKT signaling pathways. *Biomed Pharmacother* 2017; **93**: 130–145.
39. Landry NM, Cohen S, Dixon IMC. Periostin in cardiovascular disease and development: a tale of two distinct roles. *Basic Res Cardiol* 2017; **113**: 1–13.
40. Takeda K, Noguchi R, Kitade M, Namisaki T, Moriya K, Kawaratani H, Okura Y, Kaji K, Aihara Y, Douhara A, Nishimura N, Sawada Y, Seki K, Yoshiji H. Periostin cross-reacts with the renin-angiotensin system during liver fibrosis development. *Mol Med Rep* 2017; **16**: 5752–5758.
41. Dixon IMC, Landry NM, Rattan SG. Periostin reexpression in heart disease contributes to cardiac interstitial remodeling by supporting the cardiac myofibroblast phenotype. *Adv Exp Med Biol* 2019; **1132**: 35–41.